Journal of Marine Science and Technology

Volume 22 | Issue 5 Article 11

OFFSHORE STRUCTURAL DYNAMIC ANALYSIS CONSIDERING SOIL-STRUCTURE INTERACTION BY A COUPLED BEM AND MESHFREE METHOD

Min-Chou Tsai
Department of Marine Environment and Engineering, National Sun Yat-sen University, Kaohsiung County, Taiwan, R.O.C

Hsien Hua Lee
Department of Marine Environment and Engineering, National Sun Yat-sen University, Kaohsiung County, Taiwan, R.O.C., hhlee@mail.nsysu.edu.tw

Tinh Quoc Bui
Chair of Structural Mechanics, Department of Civil Engineering, University of Siegen, Siegen, Germany.

Chuanzeng Zhang
Chair of Structural Mechanics, Department of Civil Engineering, University of Siegen, Siegen, Germany.

OFFSHORE STRUCTURAL DYNAMIC ANALYSIS CONSIDERING SOIL-STRUCTURE INTERACTION BY A COUPLED BEM AND MESHFREE METHOD

Acknowledgements

This research has been financially supported in part by the NSC of ROC (Taiwan) under grants “NSC-101-2221-E-110- 108”. The financial support is gratefully appreciated. We would like to thank the reviewers for suggesting very constructive comments which helped improve our paper. It is greatly appreciated.

Journal of Marine Science and Technology, Vol. 22, No. 5, pp. 625-642 (2014)
DOI: 10.6119/JMST-013-1218-1

OFFSHORE STRUCTURAL DYNAMIC ANALYSIS CONSIDERING SOIL-STRUCTURE INTERACTION BY A COUPLED BEM AND MESHFREE METHOD

Min-Chou Tsai[1], Hsien Hua Lee[1], Tinh Quoc Bui[2], and Chuanzeng Zhang[2]

Key words: offshore structure-soil interaction, structure seismic motion, meshfree method, coupled MKEFG-BEM.

ABSTRACT

An investigation of dynamic offshore structure considering soil-structure interaction by a coupled approach based on boundary element and meshfree methods is presented. The moving Kriging interpolation is used for generating the shape functions because of possessing the Kronecker delta property, which makes easier in imposing the essential boundary conditions. The governing elastodynamic equations are transformed into a standard weak formulation. It is then discretized into a meshfree system of time-dependent equations, which are solved by the standard implicit Newmark time integration scheme. Numerical examples illustrating the applicability and effectiveness of the proposed method are presented and discussed in details. A two dimensional plane strain offshore-foundation model has been used for the time history analysis to compute the stresses and displacements against earthquake and wave loading considering the effect of soil-structure interaction. As a consequence, it is found that the method is very efficient and accurate for dynamic analysis compared with those of other conventional methods.

I. INTRODUCTION

The analysis of structural dynamics problems is of great importance in the field of structural mechanics and computational mechanics. Generally, the dynamic analysis needs more efforts in modeling because of acting of many different conditions of complicated external loadings than the static one. To find an exact solution to the class of dynamic problems usually is a hard way and in principle it could be reachable only with a simple loading condition and geometrical configuration. Due to many requirements of engineering applications in reality, such a task of finding a solution analytically is generally difficult and often impossible. Therefore, numerical computational methods emerge as an alternative way in finding an approximate solution. The finite element method (FEM), e.g. see [3, 16], formed into that issue and becomes the most popular numerical tool for dealing with these problems. The necessity of such numerical computational methods is nowadays unavoidable.

In the past two decades, the so-called meshfree or meshless methods, e.g. see [1, 5, 21], have emerged alternatively, where a set of scattered ''nodes'' in the domain is used instead of a set of ''elements'' or ''mesh'' as in the FEM. No meshing is generally required in meshfree methods. Note that the meshing here means different from the concept of background cells which are usually needed for performing the domain integrations. There is another concept of ''truly'' meshfree or meshless methods, in which no meshing at all including the background cells for the domain integrations is required, e.g. see [1]. In particular, the last author has developed the meshless local Petrov-Galekin (MLPG) method for analysis of static, dynamic and crack problems of nonhomogeneous, orthotropic, functionally graded materials as well as Reissner-Mindlin and laminated plates. Recently, an effective method by substantially adding an enrichment function into the traditional finite element approximation function; the extended finite element method (X-FEM), which aims at modeling of the discontinuity. The present work belongs to the meshfree scheme, and a novel meshfree method based on a combination of the classical elementfree Galerkin (EFG) method [5] and the moving Kriging (MK) interpolation is further developed for analysis of structural dynamics problems. Previously, the present method has been developed by the author for static analysis [9] and recently [8] for free vibration analysis of Kirchhoff plates. The MK interpolation-based meshfree method was first introduced by Gu [13] and its application to solid and structural me-

Paper submitted 05/01/13; revised 07/22/13; accepted 12/18/13. Author for correspondence: Hsien Hua Lee (e-mail: hhlee@mail.nsysu.edu.tw).
[1] Department of Marine Environment and Engineering, National Sun Yat-sen University, Kaohsiung County, Taiwan, R.O.C.
[2] Chair of Structural Mechanics, Department of Civil Engineering, University of Siegen, Siegen, Germany.

chanics problems is still young and more potential. Gu [13] successfully demonstrated its applicability for solving a simple problem of steady-state heat conduction. Lam *et al*. [18] introduced an alternative approach, a Local Kriging (LoKriging) method to two-dimensional solid mechanics problems, where a local weak-form of the governing partial differential equations was appplied. Li *et al*. [20] further developed the LoKriging method for structural dynamics analysis. Furthermore, Tongsuk *et al*. [28, 29] and Sayakoummane *et al*. [27] recently illustrated the applicability of the method to investigations of solid mechanics problems and shell structures, respectively. Imposing essential boundary conditions is a key issue in meshfree methods because of the lack of the Kronecker delta property and, therefore, the imposition of prescribed values is not as straightforward as in the FEM. Thus, many special techniques have been proposed to avoid such difficulty by various ways e.g. Lagrange multipliers [5], penalty method [21], or coupling with the FEM [5, 27], etc. Due to the possession of the Kronecker delta property, the present method is hence capable of getting rid of such drawback of enforcing the essential boundary conditions. Note here that a majority of meshfree methods has been developed by displacement-based approaches and, in contrast, The author have also implemented an equilibrium-based meshfree method for elastostatic problems where a stress-based approach is taken into consideration, see [7, 10]. With respect to the linear structural dynamics analysis in two dimensions, a variety of studies has been reported so far. Gu *et al*. [14] successfully used the meshless local Petrov-Galerkin (MLPG) method for free and forced vibration analyses for solids, while in a similar manner Hua Li *et al*. [20] developed the LoKriging, Dai and Liu [12] proposed the smoothed finite element method (SFEM), Gu and Liu [15] presented a meshfree weak-strong form (MWS) approach. As mentioned above, the proposed method has a significant advantage in the treatment of the boundary conditions, which is easier than the classical EFG. This present work essentially makes use of that good feature to structural dynamics analysis. At the standing point of view and to the best knowledge of the authors, such a task has not yet been carried out while this work is being reported. The paper is organized as follows. The moving Kriging shape function is introduced in the second section. The governing equations and their discretization of elastodynamic problems considering soil-structure interaction will then be presented in Section 3. In Section 4, the coupled MKEFG-BEM is introduced in detail. In Section 5, several studies have been carried out on the seismic responses of offshore structures. Wolf [31] first presented the direct method of soil-structure interaction analysis. Using this method the soil region near the structure along with the structure is modeled directly and he idealized soil-structure system was analyzed in a single step. Bode [6] presented a pure time domain approach is developed for analyzing general soil-structure interaction based on transient Green's functions. A zero mean ergodic Gaussian process of finite duration [24] or Kanai-Tajimi power spectrum [4, 33] was used to determine horizontal ground acceleration due to earthquakes. Two primary techniques can be used to analyze the structure-foundation system and its characteristics, direct and substructure methods, both of which are outlined by Wolf [32]. Aydinoglu [2] developed mathematical formulations for both methods. Three sub-schemes have been developed for the dynamic interactions of soil and pile groups on the seabed: the equivalent single pile scheme, the elasticity scheme, and the general threedimensional load transfer scheme. References for these methods can be found in Park *et al*. [23]. Loads on the foundation due to earthquakes involve uncertainties when the dynamic characteristics are determined using time histories of the data. Thus, for accurate dynamic structure response, uncertain parameters such as seismic motions and shearwave velocities of soil may be considered using the Monte Carlo Simulation (MCS) method, which is an efficient way to detect uncertainties. Several studies of jacket structures have been reported regarding reliability evaluation of uncertain seismic motions, e.g., [17]. Numerical examples for free and forced vibration analyses are investigated and discussed in details. Finally, some conclusions from this study are given in Section 6.

II. THE MOVING KRIGING SHAPE FUNCTION

Essentially, the moving Kriging (MK) interpolation technique is similar to the moving least square (MLS) approximation. In order to approximate the distribution function $u(x_i)$ within a sub-domain $\Omega_x \subseteq \Omega$, this function can be interpolated based on all nodal values $x_i (i \in 2\ [1,n_c])$ within the sub-domain, with n being the total number of the nodes in Ω_x. The MK interpolation $u^h(x)$, $\forall x \in \Omega_x$ is frequently defined as follows [9, 13, 28, 29].

$$u^h(x) = \left[p^T(x)A + r^T(x)B \right] u(x) \tag{1}$$

or in a shorter form of

$$u^h(x) = \sum_I^n \phi_I(x) u_I = \Phi(x) u \tag{2}$$

where $u = [u(x_1)\ \ u(x_2)\ \ \cdots\ \ u(x_n)]^T$ and $\phi_I(x)$ is the MK shape function and define by

$$\Phi(x) = \phi_I(x) = \sum_j^m p_j(x) A_{jI} + \sum_k^n r_k(x) B_{kI} \tag{3}$$

The matrixes A and B are determined by

$$A = (P^T R^{-1} P)^{-1} P^T R^{-1}$$

$$B = R^{-1}(I - PA) \tag{4}$$

where, I is an unit matrix and the vector $p(x)$ is the polynomial with m basis functions

$$p(x) = \{p_1(x) \;\; p_2(x) \;\; \cdots \;\; p_m(X)\}^T \tag{5}$$

The matrix P has size $n \times m$ and represents the collected values of the polynomial basis (5) as

$$P = \begin{bmatrix} p_1(x_1) & p_2(x_1) & \cdots & p_m(x_1) \\ p_1(x_2) & p_2(x_2) & \cdots & p_m(x_2) \\ \vdots & \vdots & \ddots & \vdots \\ p_1(x_n) & p_2(x_n) & \cdots & p_m(x_n) \end{bmatrix} \tag{6}$$

and $r(x)$ in (1) is

$$r(x) = \{R(x_1, x) \;\; R(x_2, x) \;\; \cdots \;\; R(x_n, x)\} \tag{7}$$

where $R(x_i, x_j)$ is the correlation function between any pair of the n nodes x_i and x_j, and it is belong to the covariance of the field value $u(x)$: $R(x_i, x_j) = cov\,[u(x_i)\; u(x_j)]$ and $R(x_i, x) = cov\,[u(x_i)\; u(x)]$. The correlation matrix $R[R(x_i, x_j)]_{nxn}$ is explicitly given by

$$R\Big[R(x_i, x_j)\Big] = \begin{bmatrix} p_1(x_1) & p_2(x_1) & \cdots & p_m(x_1) \\ p_1(x_2) & p_2(x_2) & \cdots & p_m(x_2) \\ \vdots & \vdots & \ddots & \vdots \\ p_1(x_n) & p_2(x_n) & \cdots & p_m(x_n) \end{bmatrix} \tag{8}$$

Many different correlation functions can be used for R but the Gaussian function with a correlation parameter θ is often and widely used to best fit the model

$$R(x_i, x_j) = e^{-\theta r_{ij}^2} \tag{9}$$

where $r_{ij} = \|x_i - x_j\|$, and $\theta > 0$ is a correlation parameter. The correlation parameter has a significant effect on the solution. In this work, the quadratic basis functions $p^T(x) = [1 \;\; x \;\; y \;\; x^2 \;\; y^2 \;\; xy]$ are used for all numerical computations. Furthermore, the MK shape function in one-dimension and its first-order derivatives used in the dynamic analysis are presented in Fig. 1. One of the most important features in meshfree methods is the concept of the influence domain where an influence domain radius is defined to determine the number of scattered nodes within an interpolated domain of interest. In fact, no exact rules can be derived appropriately to all types of nodal distributions. The accuracy of the method depends on the number of nodes inside the support domain of the interest point. Therefore, the size of the support domain should be chosen by analysts somehow to ensure the convergence of the considered problems. It might also be found in the same manner as in [1, 21]. Often, the following formula is employed to compute the size of the support domain.

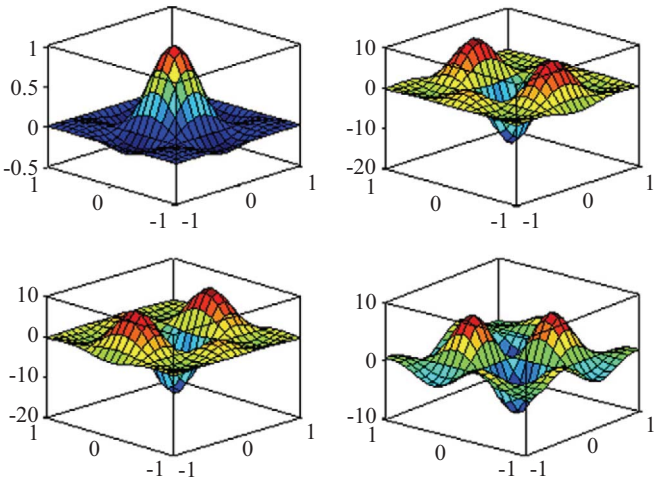

Fig. 1. The MK shape function (top-left), second-order derivatives corresponding to xx-directions (top-right), yy (bottom-left) and *xy* (bottom-right) with $p^T(x) = [1 \;\; x \;\; y \;\; x^2 \;\; y^2 \;\; xy]$.

$$d_m = \alpha d_c \tag{10}$$

where d_c is a characteristic length regarding the nodal spacing close to the point of interest, while a stands for a scaling factor shows in Fig. 2. Other features related to the method can be found in [9, 13, 28, 29] for more details.

III. MESHFREE ELASTODYNAMIC FORMULATION

1. Discrete Governing Equations

Let us consider a deformable body occupying a planar linear elastic domain Ω in a two-dimensional configuration bounded by Γ subjected to the body force b_i acting on the domain. The strong form of the initial-boundary value problems for small displacement elastodynamics with damping can be written in the form

$$\rho \ddot{u}_i + c\dot{u}_i = \sigma_{ij,j} + b_i \;\; in \;\; \Omega \tag{11}$$

where ρ stands for the mass density, c is the damping coefficient, $\ddot{u}_i$ and $\dot{u}_i$ are accelerations and velocities, and u_i specifies the stress tensor corresponding to the displacement field σ_{ij}, respectively. The corresponding boundary conditions are given as

$$u_i = \bar{u}_i \;\; \text{on the essential boundary } \Gamma_n \tag{12}$$

$$t_i = \sigma_{ij} n_j = \bar{t}_i \;\; \text{on the natural boundary } \Gamma_n \tag{13}$$

with $\bar{u}_i$ and $\bar{t}_i$ are the prescribed displacements and tractions,

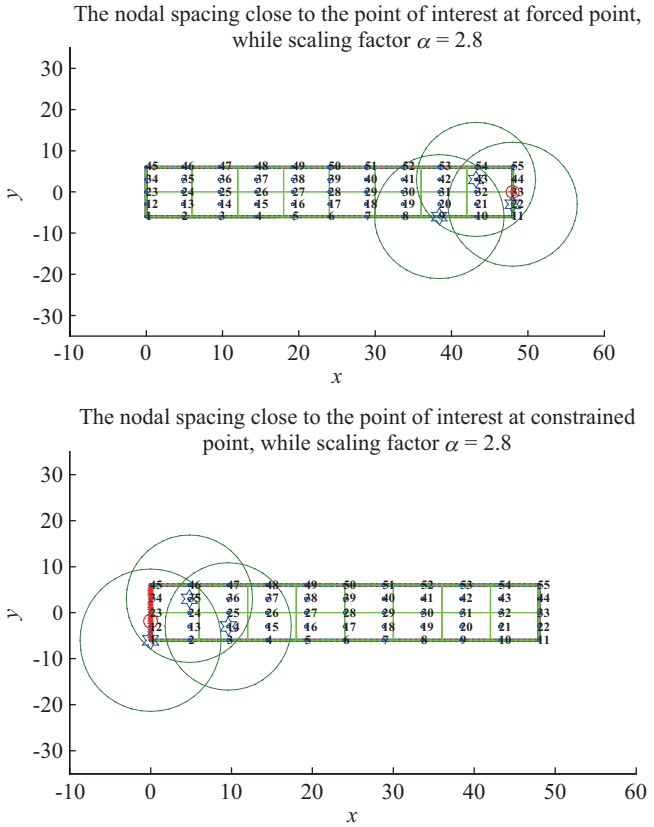

Fig. 2. Nodes whose influence domains cover the one are to be used for construction of shape functions.

respectively, and the initial conditions are defined by

$$u(x,t_0)=u_0(x),\ \ x\in\Omega \tag{14}$$

$$\dot{u}(x,t_0)=v_0(x),\ \ x\in\Omega \tag{15}$$

with u_0 and v_0 being the initial displacements and velocities at the initial time t_0, respectively, and n_j standing for the unit outward normal to the boundary $\Gamma=\Gamma_u\cup\Gamma_t$. By using the principle of virtual work, the variational formulation of the initial-boundary value problems of (11) involving the inertial and damping forces can be written as [3, 12, 16]

$$\int_\Omega \delta\varepsilon^{\mathrm{T}}\sigma d\Omega-\int_\Omega \delta u^T\left[b-\rho\ddot{u}-c\dot{u}\right]d\Omega-\int_{\Gamma_t}\delta u^T t d\Gamma=0 \tag{16}$$

In the meshfree method, the approximation (2) is utilized to calculate the displacements $u^h(x)$ for a typical point x. The discretizedform of (16) using the meshfree procedure based on the approximation (2) can be written as

$$M\ddot{u}+C\dot{u}+Ku=f \tag{17}$$

where u is known as the vector of the general nodal displacements, M, C, K and f stand for the matrixes of mass, damping and stiffness and force vector, respectively. They are defined as follows

$$M_{IJ}=\int_\Omega \Phi_I^T\rho\Phi_J d\Omega\quad C_{IJ}=\int_\Omega\Phi_I^T c\Phi_J d\Omega \tag{18}$$

$$K_{IJ}=\int_\Omega B_I^T D B_J d\Omega\quad f_I=\int_\Omega\Phi_I^T b_I d\Omega+\int_{\Gamma_t}\Phi_I^T t_I d\Gamma \tag{19}$$

where c in (18) is the damping coefficient, Φ is the MK shape function defined in (3), the elastic matrix D and the displacement gradient matrix B in (19) are given, respectively, by

$$D=\frac{E}{1-\nu^2}\begin{bmatrix}1 & \nu & 0\\ \nu & 1 & 0\\ 0 & 0 & \dfrac{(1-\nu)}{2}\end{bmatrix}(\textit{plane stress}) \tag{20}$$

$$B_I=\begin{bmatrix}\phi_{I,x} & 0\\ 0 & \phi_{I,y}\\ \phi_{I,y} & \phi_{I,x}\end{bmatrix} \tag{21}$$

2. Free Vibration Analysis

For the free vibration analysis, the damping and the external forces are not taken into account in the system. Then, (17) can be reduced to a system of homogeneous equations as [16]

$$M\ddot{u}+Ku=0 \tag{22}$$

A general solution of such a homogeneous equation system can be written as

$$u=\bar{u}e^{i\omega t} \tag{23}$$

where i is the imaginary unit, t indicates time, $\bar{u}$ is the eigenvector and ω is natural frequency or eigenfrequency. Substitution of (22) into (21) leads to the following eigenvalue equation for the natural frequency ω

$$(K-\omega^2 M)\bar{u}=0 \tag{24}$$

The natural frequencies and their corresponding mode shapes of a structure are often referred to as the dynamic characteristics of the structure.

3. Forced Vibration Analysis

For the forced vibration analysis, the approximation function (2) is a function of both space and time. For the displacements, velocities and accelerations at time $t+\Delta t$, the dynamic equilibrium equations or equations of motion presented in (17) are also considered at time $t+\Delta t$ as follows

$$M\ddot{u}_{t+\Delta t} + C\dot{u}_{t+\Delta t} + Ku_{t+\Delta t} = f_{t+\Delta t} \tag{25}$$

There are many different methods available to solve the second order time dependent problems such as Houbolt, Wilson, Newmark, Crank-Nicholson, etc. [3, 12]. In this study, the Newmark time integration scheme is adopted to solve the equations of motion expressed in (25) at time step $t + \Delta t$. The Newmark's β scheme can be given in the form [3, 16]

$$\ddot{u}_{t+\Delta t} = \frac{1}{\beta \Delta t}\left(u_{t+\Delta t} - u_t\right) - \frac{1}{\beta \Delta t}\dot{u}_t - \left(\frac{1}{2\beta} - 1\right)\ddot{u}_t$$

$$\dot{u}_{t+\Delta t} = \dot{u}_t + \left[(1-\gamma)u_t + \gamma \ddot{u}_{t+\Delta t}\right]\Delta t \tag{26}$$

By substituting both (26) into (25) one can obtain the dynamic responses at time $t + \Delta t$. Since the Newmark's β time integration scheme is an implicit method, the initial conditions of the state at $t = t_0(u_0, \dot{u}_0, \ddot{u}_0)$ are thus assumed to be known and the new state at $t_1 = t_0 + \Delta t(u_1, \dot{u}_1, \ddot{u}_1)$ is needed to be determined correspondingly. In addition, the choice of $\gamma = 0.5$ and $\beta = 0.25$, unconditionally guarantees the stability of the Newmark's β scheme with $\gamma \geq 0.5$ and $\beta \geq 0.25\,(\gamma + 0.5)^2$.

4. Mathematical Model of Coupled Offshore Structure-Soil System

In offshore structure-soil interaction problems, the foundation and the structure do not vibrate as separate systems under external excitations, rather they act together in a coupled way. Therefore, these problems have to be dealt in a coupled way. The most common SSI approach used is based on the "added motion" formulation. This formulation is mathematically simple, theoretically correct, and is easy to automate and is used with in a general linear structural analysis program. In addition, the formulation is valid for free-field motions caused by earthquake waves generated from all sources. The method requires that the free-field motions at the base of the structure be calculated before the SSI analysis. To develop the fundamental SSI dynamic equilibrium equations, the soil-structure system, as shown in Fig. 3, is considered. The absolute displacements of the structure are considered to be the sum of two parts, viz. free field displacements and added part of the displacements. Free field displacement is found out by analyzing the foundation domain with no structure present on it against the earthquake forces. The added part of the displacement is found out by carrying out coupled soil-structure interaction model. The SSI model here is divided into three sets of node points, viz. the common nodes at the interface of the structure and soil are identified with the subscript "c" (combine); the nodes with in the structure are with "s" (structure) and the nodes with in the foundation are with "f" (foundation). From the direct stiffness approach in structural analysis, the dynamic force equilibrium of the system is given in terms of the absolute displacements, *U*, by the following sub-matrix equation:

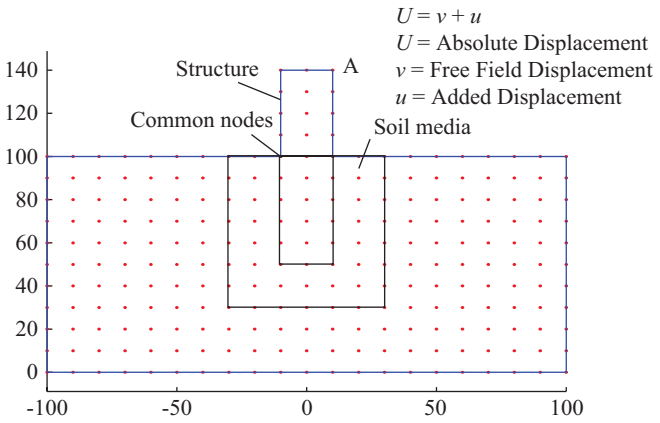

Fig. 3. Soil-structure interaction model.

$$\begin{bmatrix} M_{ss} & M_{sc} & 0 \\ M_{cs} & M_{cc} & M_{cf} \\ 0 & M_{fc} & M_{ff} \end{bmatrix} \begin{Bmatrix} \ddot{U}_s \\ \ddot{U}_c \\ \ddot{U}_f \end{Bmatrix} + \begin{bmatrix} C_{ss} & C_{sc} & 0 \\ C_{cs} & C_{cc} & C_{cf} \\ 0 & C_{fc} & C_{ff} \end{bmatrix} \begin{Bmatrix} \dot{U}_s \\ \dot{U}_c \\ \dot{U}_f \end{Bmatrix}$$

$$+ \begin{bmatrix} K_{ss} & K_{sc} & 0 \\ K_{cs} & K_{cc} & K_{cf} \\ 0 & K_{fc} & K_{ff} \end{bmatrix} \begin{Bmatrix} U_s \\ U_c \\ U_f \end{Bmatrix} = - \begin{bmatrix} M_{ss} & M_{sc} & 0 \\ M_{cs} & M_{cc} & M_{cf} \\ 0 & M_{fc} & M_{ff} \end{bmatrix} \begin{Bmatrix} \ddot{U}_s^g \\ \ddot{U}_c^g \\ \ddot{U}_f^g \end{Bmatrix} \tag{27}$$

Where the mass and stiffness at the contact nodes are the sum of the contributions from the structure (s) and foundation (f), and are given by

$$M_{cc} = M_{cc}^{(s)} + M_{cc}^{(f)} \quad C_{cc} = C_{cc}^{(s)} + C_{cc}^{(f)} \quad K_{cc} = K_{cc}^{(s)} + K_{cc}^{(f)} \tag{28}$$

In order to solve the coupled soil-structure interaction problem, we would require to solve (27). Having solved (27) using Newmark's β integration method, one would obtain the absolute displacements, velocities and accelerations of the coupled SSI problem. To avoid solving the SSI problem directly, the dynamic response of the foundation without the structure is calculated. The free-field solution is designated by the free-field displacements *v*, velocities $\dot{v}$ and accelerations $\ddot{v}$. Here, $\ddot{U}^g$ is the ground acceleration vector. By a simple change of variables, it becomes possible to express the absolute displacements *U*, velocities $\dot{U}$ and accelerations $\ddot{U}$ in terms of displacements *u*, relative to the free-field displacements *v*. Or,

$$\begin{Bmatrix} \ddot{U}_s \\ \ddot{U}_c \\ \ddot{U}_f \end{Bmatrix} = \begin{Bmatrix} \ddot{v}_s \\ \ddot{v}_c \\ \ddot{v}_f \end{Bmatrix} + \begin{Bmatrix} \ddot{u}_s \\ \ddot{u}_c \\ \ddot{u}_f \end{Bmatrix} \qquad \begin{Bmatrix} \dot{U}_s \\ \dot{U}_c \\ \dot{U}_f \end{Bmatrix} = \begin{Bmatrix} \dot{v}_s \\ \dot{v}_c \\ \dot{v}_f \end{Bmatrix} + \begin{Bmatrix} \dot{u}_s \\ \dot{u}_c \\ \dot{u}_f \end{Bmatrix}$$

$$\begin{Bmatrix} U_s \\ U_c \\ U_f \end{Bmatrix} = \begin{Bmatrix} v_s \\ v_c \\ v_f \end{Bmatrix} + \begin{Bmatrix} u_s \\ u_c \\ u_f \end{Bmatrix} \tag{29}$$

After replacing the values of, and from (29), (27) is expressed as

$$\begin{bmatrix} M_{ss} & M_{sc} & 0 \\ M_{cs} & M_{cc} & M_{cf} \\ 0 & M_{fc} & M_{ff} \end{bmatrix} \begin{Bmatrix} \ddot{u}_s \\ \ddot{u}_c \\ \ddot{u}_f \end{Bmatrix} + \begin{bmatrix} C_{ss} & C_{sc} & 0 \\ C_{cs} & C_{cc} & C_{cf} \\ 0 & C_{fc} & C_{ff} \end{bmatrix} \begin{Bmatrix} \dot{u}_s \\ \dot{u}_c \\ \dot{u}_f \end{Bmatrix}$$

$$+ \begin{bmatrix} K_{ss} & K_{sc} & 0 \\ K_{cs} & K_{cc} & K_{cf} \\ 0 & K_{fc} & K_{ff} \end{bmatrix} \begin{Bmatrix} u_s \\ u_c \\ u_f \end{Bmatrix} = R + F \tag{30}$$

where

$$R = -\begin{bmatrix} M_{ss} & M_{sc} & 0 \\ M_{cs} & M_{cc} & M_{cf} \\ 0 & M_{fc} & M_{ff} \end{bmatrix} \begin{Bmatrix} \ddot{v}_s \\ \ddot{v}_c \\ \ddot{v}_f \end{Bmatrix} - \begin{bmatrix} C_{ss} & C_{sc} & 0 \\ C_{cs} & C_{cc} & C_{cf} \\ 0 & C_{fc} & C_{ff} \end{bmatrix} \begin{Bmatrix} \dot{v}_s \\ \dot{v}_c \\ \dot{v}_f \end{Bmatrix}$$

$$- \begin{bmatrix} K_{ss} & K_{sc} & 0 \\ K_{cs} & K_{cc} & K_{cf} \\ 0 & K_{fc} & K_{ff} \end{bmatrix} \begin{Bmatrix} v_s \\ v_c \\ v_f \end{Bmatrix} \tag{31}$$

$$F = -\begin{bmatrix} M_{ss} & M_{sc} & 0 \\ M_{cs} & M_{cc} & M_{cf} \\ 0 & M_{fc} & M_{ff} \end{bmatrix} \begin{Bmatrix} \ddot{U}_s^g \\ \ddot{U}_c^g \\ \ddot{U}_f^g \end{Bmatrix} \tag{32}$$

This is a numerically cumbersome approach; hence, an alternative approach is necessary to formulate the solution directly in terms of the absolute displacements of the structure. Since the analysis is now for the foundation part only (free field analysis), hence the corresponding values of the displacement, velocity and acceleration for the structural part is taken as zero. This involves the introduction of the following change of variables:

$$\begin{Bmatrix} \ddot{U}_s \\ \ddot{U}_c \\ \ddot{U}_f \end{Bmatrix} = \begin{Bmatrix} 0 \\ \ddot{v}_c \\ \ddot{v}_f \end{Bmatrix} + \begin{Bmatrix} \ddot{u}_s \\ \ddot{u}_c \\ \ddot{u}_f \end{Bmatrix} \qquad \begin{Bmatrix} \dot{U}_s \\ \dot{U}_c \\ \dot{U}_f \end{Bmatrix} = \begin{Bmatrix} 0 \\ \dot{v}_c \\ \dot{v}_f \end{Bmatrix} + \begin{Bmatrix} \dot{u}_s \\ \dot{u}_c \\ \dot{u}_f \end{Bmatrix}$$

$$\begin{Bmatrix} U_s \\ U_c \\ U_f \end{Bmatrix} = \begin{Bmatrix} 0 \\ v_c \\ v_f \end{Bmatrix} + \begin{Bmatrix} u_s \\ u_c \\ u_f \end{Bmatrix} \tag{33}$$

In order to calculate the free field displacements *v*, only foundation domain is solved by considering no structure is present on it. The foundation domain is subjected to earthquake motion and the free-field displacement for the common and other foundation nodes are obtained.

$$\begin{bmatrix} M_{cc} & M_{cf} \\ M_{fc} & M_{ff} \end{bmatrix} \begin{Bmatrix} \ddot{v}_c \\ \ddot{v}_f \end{Bmatrix} + \begin{bmatrix} C_{cc} & C_{cf} \\ C_{fc} & C_{ff} \end{bmatrix} \begin{Bmatrix} \dot{v}_c \\ \dot{v}_f \end{Bmatrix} + \begin{bmatrix} K_{cc} & K_{cf} \\ K_{fc} & K_{ff} \end{bmatrix} \begin{Bmatrix} v_c \\ v_f \end{Bmatrix}$$

$$= -\begin{bmatrix} M_{cc} & M_{cf} \\ M_{fc} & M_{ff} \end{bmatrix} \begin{Bmatrix} \ddot{U}_c^g \\ \ddot{U}_f^g \end{Bmatrix} \tag{34}$$

After obtaining the free field response (i.e. v, $\dot{v}$ and $\ddot{v}$) the interaction force R is calculated using (35) in the following simplified manner:

$$R = -\begin{bmatrix} M_{ss} & M_{sc} & 0 \\ M_{cs} & M_{cc}^{s} & 0 \\ 0 & 0 & 0 \end{bmatrix} \begin{Bmatrix} 0 \\ \ddot{v}_c \\ 0 \end{Bmatrix} - \begin{bmatrix} C_{ss} & C_{sc} & 0 \\ C_{cs} & C_{cc} & 0 \\ 0 & 0 & 0 \end{bmatrix} \begin{Bmatrix} 0 \\ \dot{v}_c \\ 0 \end{Bmatrix}$$

$$- \begin{bmatrix} K_{ss} & K_{sc} & 0 \\ K_{cs} & K_{cc} & 0 \\ 0 & 0 & 0 \end{bmatrix} \begin{Bmatrix} 0 \\ v_c \\ 0 \end{Bmatrix} \tag{35}$$

After obtaining the interaction forces R, the added responses of the dam and foundation domain are calculated using (36). And then the added responses (i.e. u, $\dot{u}$ and $\ddot{u}$) are added to the free field responses to get the absolute responses of the coupled soil and structure domain, following (33):

$$\begin{bmatrix} M_{ss} & M_{sc} & 0 \\ M_{cs} & M_{cc} & M_{cf} \\ 0 & M_{fc} & M_{ff} \end{bmatrix} \begin{Bmatrix} \ddot{u}_s \\ \ddot{u}_c \\ \ddot{u}_f \end{Bmatrix} + \begin{bmatrix} C_{ss} & C_{sc} & 0 \\ C_{cs} & C_{cc} & C_{cf} \\ 0 & C_{fc} & C_{ff} \end{bmatrix} \begin{Bmatrix} \dot{u}_s \\ \dot{u}_c \\ \dot{u}_f \end{Bmatrix}$$

$$+ \begin{bmatrix} K_{ss} & K_{sc} & 0 \\ K_{cs} & K_{cc} & K_{cf} \\ 0 & K_{fc} & K_{ff} \end{bmatrix} \begin{Bmatrix} u_s \\ u_c \\ u_f \end{Bmatrix} = R + F \tag{36}$$

The main assumptions used in this model are that the input motions at the level of the base rock are not considered to be affected by the presence of the offshore structure and that all interface nodes will be subjected to the same free-field accelerogram. In theory any desired spatial variation of the free-field components could be considered at the interface, but there is seldom sufficient information to specify such variation. In this case, the mass of the foundation is taken into account in the analysis such that it will represent the offshore structure-soil interaction in a relatively more realistic manner. The effect of hydrodynamic pressure is considered according to added mass technique originally proposed by Westergaard [29]. Assuming the sea water to be inviscid and incompressible and its motion to be of small amplitude, the governing equation for hydrodynamic pressure is expressed as

$$\nabla^2 p = 0 \tag{37}$$

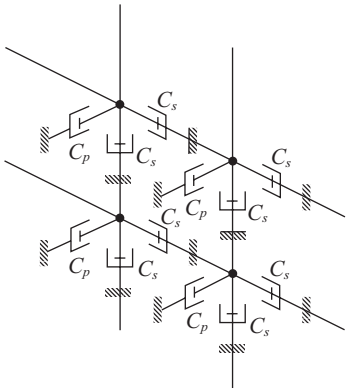

Fig. 4. Viscous dashpots connected to each degrees of freedom of a boundary node.

The solution of this equation is proposed by Westergaard [29] and is used in the present work to calculate the hydrodynamic pressure imposed on the interface of the pile body during any earthquake.

5. Absorbing Boundary

A way to eliminate seismic waves propagating outward from the structure is to use Lysmerand Kuhlemeyer [22] boundaries. This method consists of simply connecting dashpots to all degrees of freedom of the boundary nodes and fixing them on the other end Fig. 4. Lysmerand Kuhlemeyer [22] boundaries are derived for an elastic wave propagation problem in one-dimensional semi- infinite bar. The damping coefficient C of the dashpot equals

$$C = A\rho c \tag{38}$$

where A is the cross section of the bar, r is the mass density and c is the wave velocity that has to be selected according to the type of wave that has to be absorbed (shear wave velocity c_s or compression wave velocity c_p). In two dimensions (38) takes the following form, which results in damping coefficient C_n and C_t in the normal and tangential direction, respectively.

$$C_n = A_1\rho c_p$$

$$C_t = A_2\rho c_s \tag{39}$$

The shear wave velocity c_s and compression wave velocity c_p is given by

$$c_s = \sqrt{\frac{G}{\rho}}$$

$$c_p = \sqrt{\frac{E(1-\nu)}{(1+\nu)(1-\nu)\rho}} \tag{40}$$

Where G is the shear modulus of the medium and is expressed as

$$G = \frac{E}{2(1+\nu)} \tag{41}$$

The E is the Young's modulus and v is Poisson's ratio. However, in general, the directions of the incident waves are not known in advance. In these cases, it's advantageous to use a 'diffused' version as suggested by White *et al*. [31]. Assuming that the wave energy arrives at the boundary with equal probability from all directions, effective factors A_1 and A_2 are evaluated by minimizing the ratio between the reflected energy and the incident energy over the range of incident angles. For an isotropic medium this results in

$$A_1 = \frac{8}{15\pi}(5+2S-2S^2)$$

$$A_2 = \frac{8}{15\pi}(3+2S^2)$$

$$S = \sqrt{\frac{(1-2\nu)}{2(1-\nu)}} \tag{42}$$

6. Morison's Equation

The Morison's equation is widely used to estimate fluid force acting on a submerged object. If the velocity and the acceleration of fluid are given at the representing position of the object, it is easy to evaluate wave force including drag and inertia terms based on an empirical equation [11]. The equation includes two coefficients such as C_D and C_M corresponding to the drag and the inertia force respectively. Those coefficients can be fixed based on the shape of the object. The Morison's equation is as shown in (43).

$$F_w = \frac{1}{2}\rho A C_D u|u| + \rho V C_M \frac{du}{dt} \tag{43}$$

$$\{F_w\} = [C_M]\{\dot{v}\} - [C_M]\{\ddot{u}\} + [C_D]\{|\dot{v}-\dot{u}|(\dot{v}-\dot{u})\}$$

$$[C_M] = \begin{bmatrix} \ddots & & \\ & \rho C_M V & \\ & & \ddots \end{bmatrix}; [C_D] = \begin{bmatrix} \ddots & & \\ & \rho C_D \frac{A}{2} & \\ & & \ddots \end{bmatrix} \tag{44}$$

F_w: fluid wave force, C_D: drag force coefficient, C_M: inertia force coefficient, u: velocity of fluid, A: area of member, V: volume of member.

A survey of measured values for C_D and C_M made by the British Ship Research Association (1976) is depicted in Fig. 5.

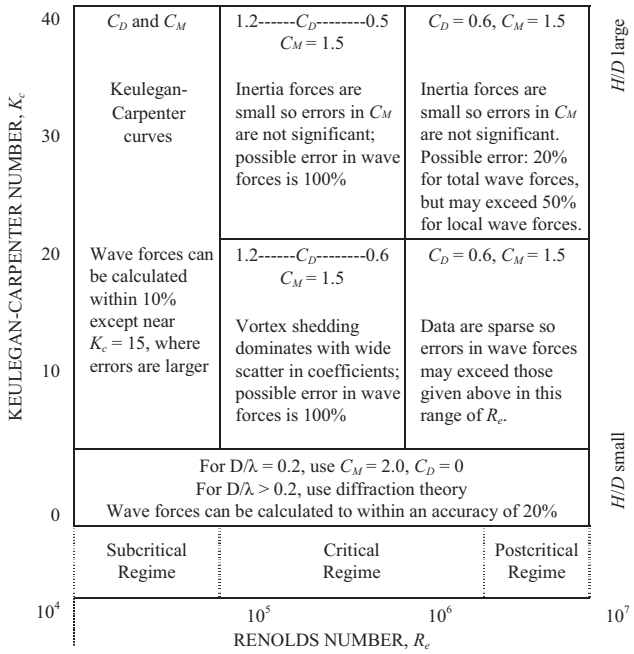

Fig. 5. Summary of C_D and C_M for smooth, vertical cylinders (British Ship Research Association, 1976).

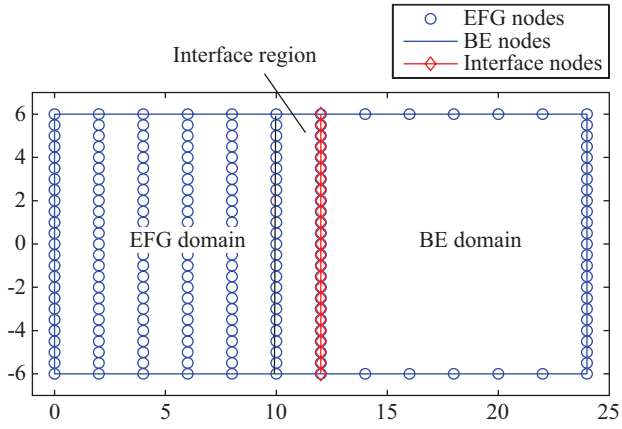

Fig. 6. Coupling of an EFG and a BE subdomain.

IV. COUPLING EFGM WITH MESH-BASED METHODS

1. Coupled EFGM-BEM

To couple the EFGM with BEM, interface element similar to those used in the EFGM-FEM coupling have been developed Liu [21], Fig. 6 illustrates a typical situation involving the EFGM and the BEM.

Since the BE shape functions adopt the same from as the FE ones, along the interface Γ_I, compatibility and equilibrium condition must be satisfied simultaneously. The nodal displacements and the nodal forces along Γ_I, for Ω_1 (EFG domain) and for Ω_2 (BEM domain), must be equal and sum up to zero. The construction procedure of the interface element can be shown as

$$u_I^1 = u_I^2$$

$$F_I^1 + F_I^2 = 0 \tag{45}$$

The modified displacement approximation in Ω_I (Interface region) and the remaining part of Ω_1 have the form

$$u_i^h(x,t) = \begin{cases} \left[1 - R(x)\right] u_i^{BE}(x,t) + R(x) u_i^{EFG}(x,t), x \in \Omega_I \\ R(x) u_i^{EFG}(x,t), x \in \Omega_1 - \Omega_I \end{cases} \tag{46}$$

where $u_i^h(x,t)$ is the displacement of a point in Ω_1, and $u_i^{EFG}(x,t)$ is the EFG displacement given by

$$u^{EFG} = \sum_{I=1}^{n} \phi_I(x) u_I(t) \tag{47}$$

φ_I are the MK shape defined by (3), and collocation the $u^{BE}(x, t)$ at each boundary node at all n time-steps leads to the system of equations

$$U^1 s^n = T^1 u^n + \sum_{m=1}^{n-1} \left[T^{n-m+1} u^m - U^{n-m+1} s^m \right] \tag{48}$$

m is the number of time basis functions and n is the number of field nodes included in the support domain of the point x, in which U^i and T^i are influence matrices whose coefficients are the integral terms evaluated over each boundary point and over the time $i\Delta t$; the vectors u^m and s^m contain the nodal values of the displacements and tractions, respectively.

2. Treatments at the Interface

From the EFGM nodal forces are obtained, while surface tractions are used in the BEM. In order to reach consistency between the EFG and the BE formulations, the traction vector s obtained from the BE system of equations (48) has to be transformed to a force vector F_{BE} by means of a transformation matrix M_t, such that

$$F_{BE} = M_t \cdot s \tag{49}$$

The transformation matrix M_t can be evaluated by the BE shape functions N_i. Along the boundary of an interface element Γ_e the ij-th element of the matrix M_t is caculated by

$$M_t(i,j) = \int_{\Gamma_e} N_i N_j d\Gamma \tag{50}$$

Using (49), a global nodal force vector can be formulated, which relates the BE nodal forces to the displacements at the

current time-step n and a sum of the influence of all previous time-steps (m = 1, 2, 3, …, n-1):

$$F_{BE}^{n} = M_t \left[U^1\right]^{-1} T^1 u^n + M_t \left[U^1\right]^{-1} \sum_{m=1}^{n-1} \left[T^{n-m+1} u^m - U^{n-m+1} M_t^{-1} F^m\right]$$

$$= K_{BE} u^n + \sum_{m=1}^{n-1} H_m^n$$

$$= R_{BE}^n + \sum_{m=1}^{n-1} H_m^n \tag{51}$$

The vector H in (51) contains the nodal force contribution from all previous time-steps. Therefore, it is known at the time-step m. For two-dimensional problems, in soil-structure interaction elastic waves play a significant role. The Lame-Navier equation

$$(\lambda + \mu) u_{i,ij} + \mu u_{j,ii} + \rho(b_j - \ddot{u}_j) = 0 \tag{52}$$

ρ is the mass density of the solid body, b_j are components of the body force per unit volume, the Lame constant λ and μ are defined as

$$\mu = G = \frac{E}{2(1+\nu)} \quad \lambda = \frac{E\nu}{(1+\nu)(1-2\nu)} \tag{53}$$

where G and E are the shear and Young's modulus, respectively. N is the Poisson's ratio. The constant parameters represent the dilatational and shear wave velocity, respectively.

$$c_p = \sqrt{\frac{\lambda + 2\mu}{\rho}} \quad c_s = \sqrt{\frac{\mu}{\rho}} \tag{54}$$

With the definition, the Lame-Navier equation can be written as

$$(c_p^2 - c_s^2) u_{i,ij} + c_s^2 u_{j,ii} + \rho(b_j - \ddot{u}_j) = 0 \tag{55}$$

This is the well known wave equation in elastodynamics. While in general the EFGM is able to model the nonlinear behavior of a structural system, the BEM is usually restricted to the investigation of linear elastic systems. Thus, in the coupling process, which shall be used to consider linear as well as nonlinear problems, equilibrium has to be ensured during the integration of the linear BEM equation.

3. Coupling Procedure

In each time-step equilibrium needs to be satisfied before continuing with the time marching scheme. Flow chart shows in Fig. 7. For the coupled system of equations, this means that the residual force at the k-th step of the $\Psi(u_k)$, give by

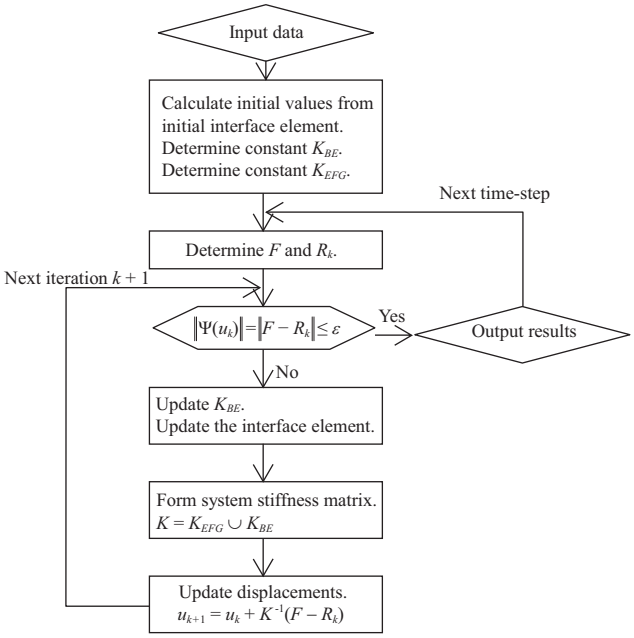

Fig. 7. Flow chart of the EFGM-BEM for a nonlinear dynamic analysis.

$$\left\|\Psi(u_k)\right\| = \left\|F - R_k\right\| \tag{56}$$

should vanish or at least be very small. The vectors F and R_k comprise the EFG as well as the BE part which can be determined by (57), (58), respectively.

$$F_{eff} = F^n - R_k^n + M\left(\frac{4}{\Delta t^2} u_{k+1}^{n-1} + \frac{4}{\Delta t} \dot{u}_{k+1}^{n-1} + \ddot{u}_{k+1}^{n-1}\right) \tag{57}$$

$$R_{eff} = K_{eff} \Delta u_{k+1}^n + M \frac{4}{\Delta t^2} u_k^n \tag{58}$$

The global stiffness matrix of the coupled system can be derived by

$$K = \frac{\partial \Psi}{\partial u} = K_{EFG} \cup K_{BE} \tag{59}$$

where K_{EFG} takes the form of K_{eff} defined in (60) when an nonlinear analysis is carried out. As the stiffness matrix of the BE part K_{BE} is not dependent on the time, only the stiffness matrix of the EFG part K_{EFG}, and the consequently constructed interface elements, have to be updated at each time-step. The update of the displacement in the coupled system can be expressed by

$$K_{eff} = K + \frac{4}{\Delta t^2} M \tag{60}$$

The iteration will not cease until the different between F and R_k predefined small value (error limit).

Table 1. Comparison of the natural frequencies for different node distributions for the cantilever beam.

Mode (Hz)	FEM [20] (4850DOF)	55 Nodes			189 Nodes		
		LoKriging [20]	Present	error (%)	LoKriging [20]	Present	error (%)
1	27.72	28.16	27.952	0.8369	27.76	27.781	0.2200
2	140.86	142.94	143.943	2.1886	140.46	142.525	1.1820
3	179.71	178.90	179.874	0.0912	178.81	179.781	0.0395
4	323.89	329.08	334.562	3.2949	323.83	331.385	2.3140
5	523.43	529.77	537.394	2.6677	523.96	538.608	2.8997
6	536.57	535.58	548.201	2.1676	534.12	542.063	1.0237
7	730.04	733.34	776.301	6.3367	731.11	763.999	4.6516
8	881.28	882.40	884.231	0.3348	877.89	888.505	0.8198
9	899.69	902.75	929.177	3.2774	899.46	921.521	2.4265
10	1000.22	1001.55	1046.214	4.5983	999.39	1028.855	2.8628

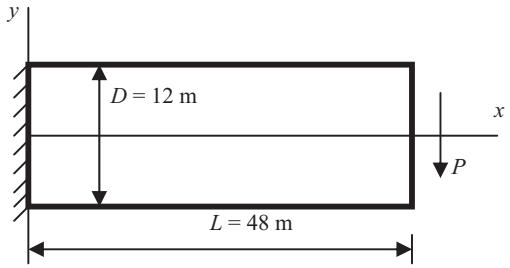

Fig. 8. The geometry of the cantilever beam. for free vibration analysis and static analysis subjected to a parabolic traction at the free end P = -1000 N.

$$u_{k+1} = u_k + K^{-1}(F - R_k) \tag{61}$$

V. NUMERICAL RESULTS

In order to demonstrate the efficiency and the applicability of the present method to analysis of structural dynamics problems, A typical numerical examples are considered for free and forced vibrations and their dynamic responses are reported correspondingly.

1. Static and Free Vibration Analysis

A cantilever beam as shown in Fig. 8 is first considered as a benchmark example. To do so, the non-dimensional parameters in the computation have the length L = 48 m and height D = 12 m. The beam is assumed to have a unit thickness so that plane stress condition is valid. Young's modulus E = 3.0×10^7 (kN/m^2), Poisson's ratio ν = 0.3, and mass density ρ = 1.0 (kN/m^3) [9] are used. As confirmed by static analysis in the previous work [9], two important parameters involving the correlation coefficient θ and the scaling factor α related to the interpolation function expressed in (9) and (10), respectively; have certain influences on the numerical solutions. Thus, they are of importance to the present method and may also have effects on the dynamic analysis in the present work. This implies that the choice of these two parameters must be in carefulness, and the choice might be different from the static analysis. The correlation parameter is varied in an interval of $0.004 < \theta < 1000$ whilst $\alpha = 2.8$ is fixed. A regular set of 189 scattered nodes is taken in this example and its distribution will be seen later. A comparison of the obtained results of the present method to that of the LoKriging [20] and the FEM (4850 DOFs) [20] is given in Table 1 below. Fig. 9 shows the computed results of the natural frequency of the beam compared to those of available reference solutions. It is found that a good agreement can be reached if $0.004 \le \theta < 5$ is chosen, it fails with $0 \le \theta < 0.004$, and other θ values are though possible but the error increases and a bad result is unavoidable. Fig. 10 note that the FEM (4850 DOFs) derived from [20] is used as a reference solution for the verification purpose. The correlation coefficient θ= 0.2 is kept unchanged in the computation. Definitely, a smaller error is obtained with a scaling factor $2.4 \le \alpha \le 3.0$. For static analysis the traction is distributed in a form of parabola at the right end of the beam. Strain energy error e is employed as an indicator of accuracy of the MK-EFG numerical results in (62)

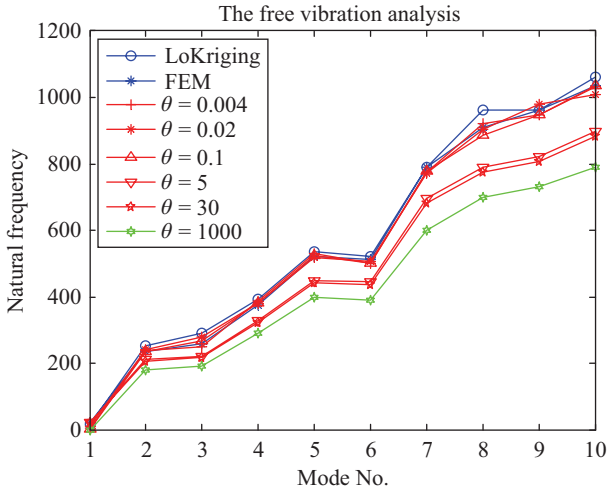

Fig. 9. Natural frequency versus the correlation parameter θ for the cantilever beam (α = 2.8).

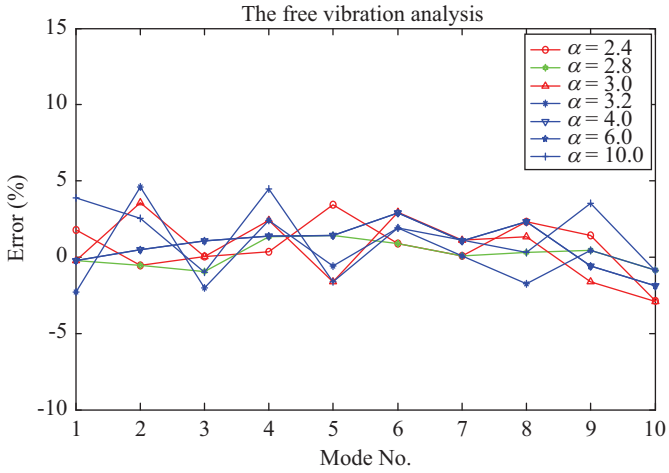

Fig. 10. Influence of scaling factor α on the natural frequency (θ = 0.2).

$$e_e = \left[\frac{1}{2}\int_\Omega (\varepsilon^{num} - \varepsilon^{exact}) D (\varepsilon^{num} - \varepsilon^{exact}) d\Omega\right]^{1/2} \qquad (62)$$

Fig. 11(a) shows the exact and numerical solutions of MK-EFG for the distribution of stress σ_{xx} on the cross section of $x = L/2$ of the cantilever beam. The plot shows excellent agreement between the exact solution and the numerical results for all the parameters of θ and α used. A very coarse mesh can yield good results. Errors in stress between the exact solution and the numerical results are clearly evident. This fact implies that the stresses that are obtained using the derivatives of the displacement field are very sensitive to the way the integration is performed. Fig. 11(b) and (c) show, respectively, the stress components σ_{yy} and σ_{xy}. It is clearly shown again that the stresses are very sensitive with the chosen parameters of θ and α, especially the shear stress σ_{xy}.

Table 1 listing the first ten frequencies shows a comparison of natural frequencies among LoKriging [20], FEM (4850 DOFs) [20] and the present method, in which two scattered nodes of coarse and fine node distributions with 55 and 189 are considered for the cantilever beam associated with the chosen parameters of θ = 0.2 and α = 3.0. An excellent agreement with other solutions can be found. Furthermore, the first nine eigenmodes of the cantilever beam are also provided in Fig. 12.

To analyze the influences of the density of nodal distributions and the convergence of the natural frequencies versus the nodal densities, five regular nodal distributions with 5 × 5; 11 × 5; 15 × 9; 21× 9 and 21 × 16 are additionally applied to the beam problem and four of them are illustrated in Fig. 13.

The corresponding results of the non-dimensional frequencies are calculated individually for each set of scattered nodes and presented in Table 2 in comparison with those obtained by LoKriging [20] and the FEM [20]. It shows a very good convergence of the frequencies to the reference solutions even with a coarse set of 55 nodes. For quantitative analysis, the following norm is defined as the error indicator.

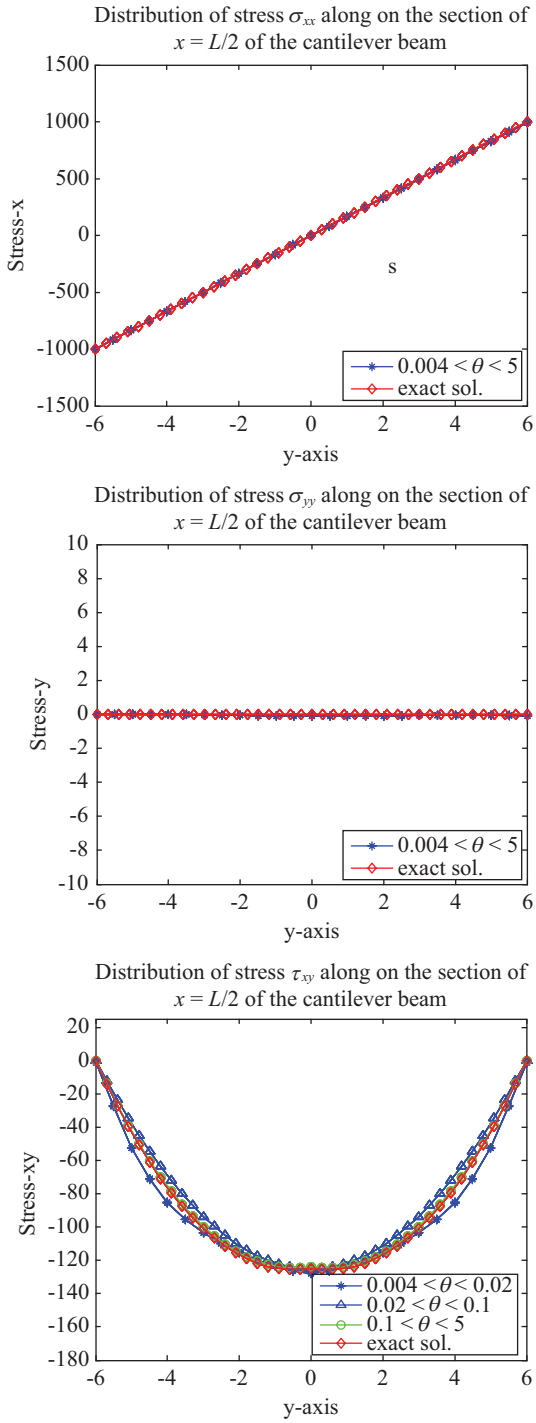

Fig. 11. Influence of correlation parameter θ (a) σ_{xx} (b) σ_{yy} (c) τ_{xy} distributions on the cross-section of the beam at $x = L/2$, 0.004 < θ <5, α = 2.8.

$$error(\%) = \frac{Mode\_No.^{num} - Mode\_No.^{FEM}}{Mode\_No.^{FEM}} \qquad (63)$$

The next numerical example dealing with a offshore structure-soil system as shown in Fig. 14 is considered. The

Table 2. Convergence of the natural frequencies (Hz) with various nodal densities of the cantilever beam.

Mode	5 × 5	11 × 5	15 × 9	21 × 9	21 × 16	LoKriging [20]	FEM [20]
1	31.384	27.952	27.648	27.781	27.725	27.76	27.72
2	149.236	143.943	142.474	142.525	141.770	140.46	140.86
3	162.053	179.874	179.653	179.781	179.433	178.81	179.71
4	314.614	334.562	331.419	331.385	324.355	323.83	323.89
5	326.115	537.394	538.284	538.608	524.267	523.96	523.43
6	365.320	548.201	545.519	542.063	537.306	534.12	536.57
7	551.751	776.301	765.665	763.999	738.306	731.11	730.04
8	1112.647	894.231	889.478	888.505	884.180	877.89	881.28
9	1209.457	929.177	925.343	921.521	899.173	899.46	899.69
10	1369.263	1046.214	1032.822	1028.855	1002.132	999.39	1000.22

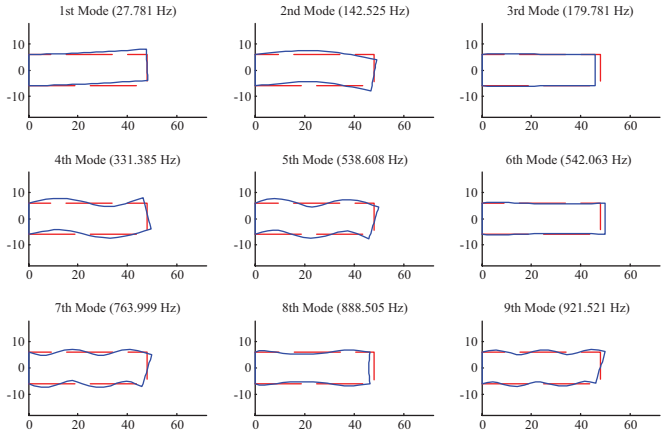

Fig. 12. The first nine eigen-modes of the cantilever beam by the present method.

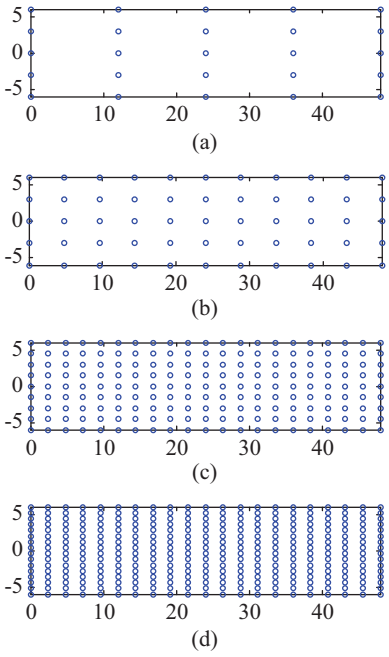

Fig. 13. Various regular nodal distributions: (a) 5 × 5, (b) 11 × 5, (c) 21 × 9 and (d) 21 × 16.

Table 3. Structural properties of the offshore platform with a pile-soil foundation system.

Description	Value	Unit
Deck size	48	m
Number of columns	2	-
Column center to center distance	24	m
Column outer diameter	12	m
Column height	39	m
Truss structure height	39	m
Middle pipe diameter of truss structure	1	m
Small pipe diameter of truss structure	0.5	m
Deck weight	4	mN
Structure weight per unit volume	77	kN/m^3
Young's modulus	3.0×10^7	kN/m^2
Stiffness per unit length	1.0×10^7	kN/m
Number of piles	2	-
Length of pile	39	m
Diameter of pile	0.6	m
Density of soil	1.7	ton/m^3
Poisson's ratio of soil	0.4	-

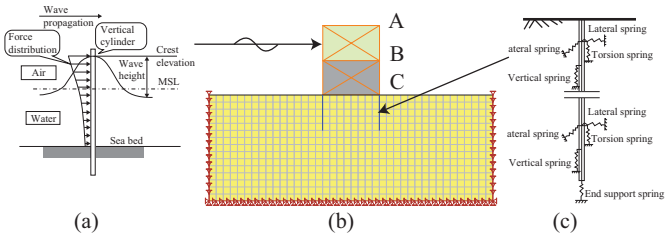

Fig. 14. The geometry of offshore structure-soil prototype. (a) Wave force distribution. (b) All side boundary nodes are fitted with dashpots in both tangential and horizontal directions. (c) Pile-soil interface spring system.

offshore structure -soil system has been solved using several different computational methods such as MCS method [23]. The geometrical parameters of the offshore structure -soil system can be found in Table 3 and other relevant material parameters are taken exactly the same as in Table 3. The first

Table 4. Natural periods of the present platform for various soil conditions (sec).

Mode (sec)	Vs = 100 m/s		Vs = 300 m/s		Vs = 500 m/s		Fixed	
	MCS*	MF**	MCS*	MF**	MCS*	MF**	MCS*	MF**
1	2.647	2.773	2.389	2.456	2.341	2.395	2.056	2.122
2	2.578	2.654	2.279	2.312	2.244	2.298	2.045	2.079
3	2.498	2.523	2.221	2.279	2.176	2.205	1.937	2.001
4	1.150	1.198	1.072	1.132	1.063	1.088	0.983	1.012
5	0.576	0.596	0.536	0.579	0.529	0.565	0.516	0.532

* Monte Carlo Simulation method (FE modal)

** Present method (MFree modal)

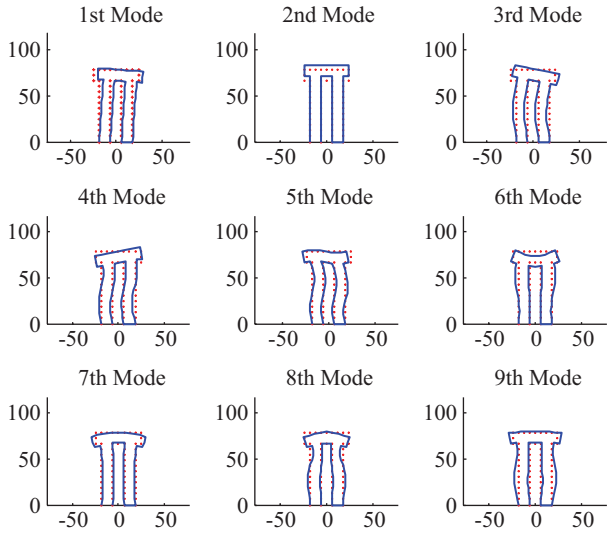

Fig. 15. The first nine eigen-modes of the offshore structure by the present method.

five natural frequencies are given in Table 4. Two sets of 126 and 393 scattered nodes are used, as well as $\theta = 0.2$ and $\alpha = 3.0$ are specified in the computation as shown in Fig. 16. As a consequence, it is found that the present solutions are in a good agreement with the ones obtained by BEM, FEM. Additionally, the first nine eigenmodes are also presented in Figs. 15 and 17 for the offshore structure-soil system.

2. Forced Vibration Analysis

Regarding the analysis of the forced vibration, the same cantilever bean and offshore structure-soil system in two-dimensional setting are chosen. At first, the composite beam is considered to be in plane stress condition with parameters $E_1 = 3 \times 10^7$ (kN/m^2), $E_2 = 3 \times 10^6$ (kN/m^2), $\nu = 0.3$, mass density $\rho = 1.0$ (kN/m^3), and the thickness $t = 1.0$ m, respectively. A regular set of 189 scattered nodes is used for all implementations of the forced vibration analysis. The dynamic loadings depicted as Heaviside step loading with a finite decreasing time are analyzed associated with a traction at the free end of the beam by $P = 1000\ \mathrm{N} \times g(t)$, where $g(t)$ is the time-dependent function. The implicit Newmark β time integration scheme is applied. The vertical displacement or

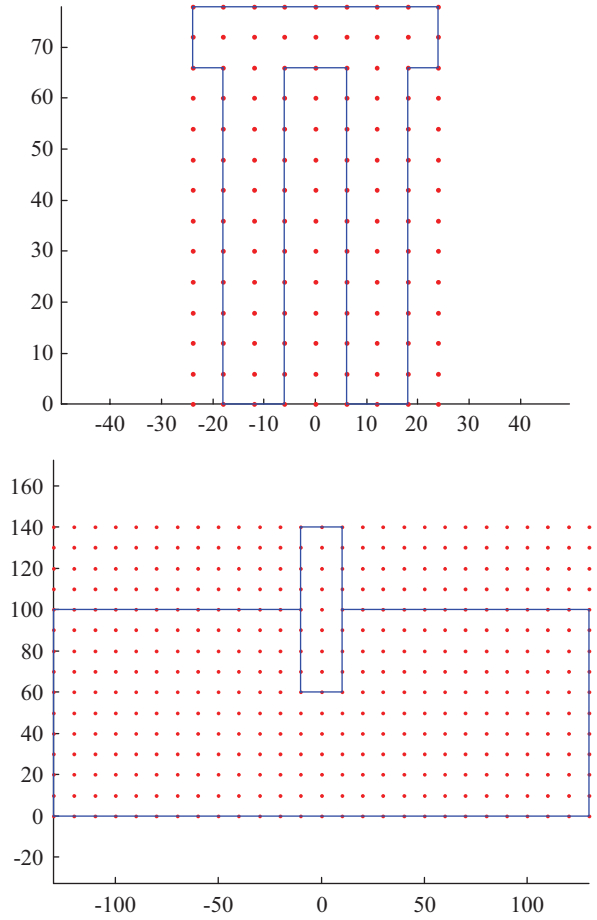

Fig. 16. Offshore structure-soil system regular nodal distributions, unit: m (a) offshore-structure with a (b) pile-soil interface spring system.

deflection at point A as depicted in Fig. 18 is computed, and the detailed results obtained by the present method are then compared either to other available solutions.

For the transient loading with a finite decreasing time as depicted in Fig. 19, the loading function is determined by (64). The corresponding results with and without damping are provided in Fig. 22, respectively. Because the input values of the problem are set up the same as that of [15, 20],

$$g(t) = (1-t)\left[H(t) - H(t-1)\right]. \tag{64}$$

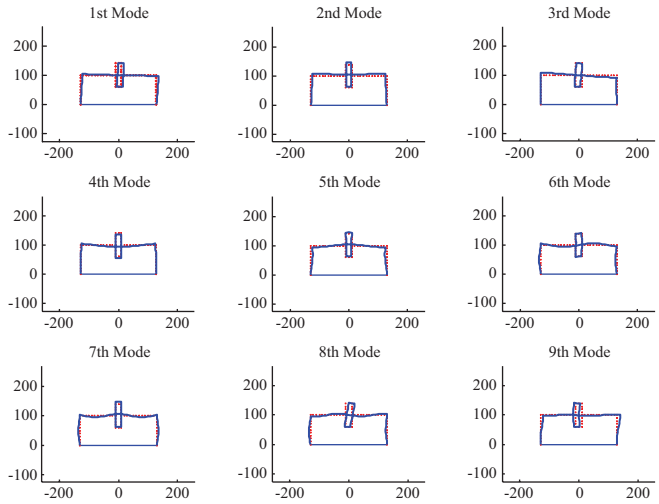

Fig. 17. The first nine eigen-modes of the offshore pile-soil interface spring system by the present method.

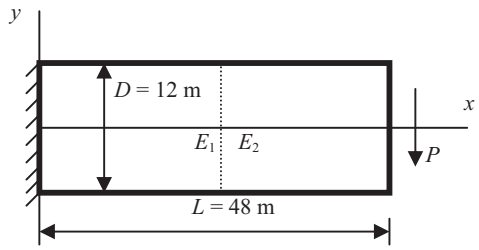

Fig. 18. A cantilever composite beam subjected to a tip uniform traction.

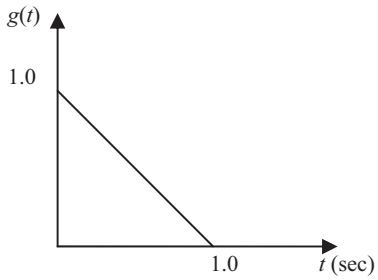

Fig. 19. Schematic diagram of dynamic transient loading with a finite decreasing time.

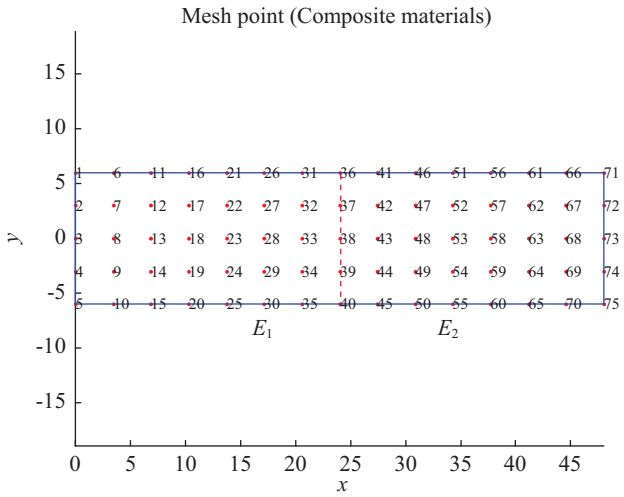

Fig. 20. Regular nodal distributions 15 × 5 for composite beam, unit: m.

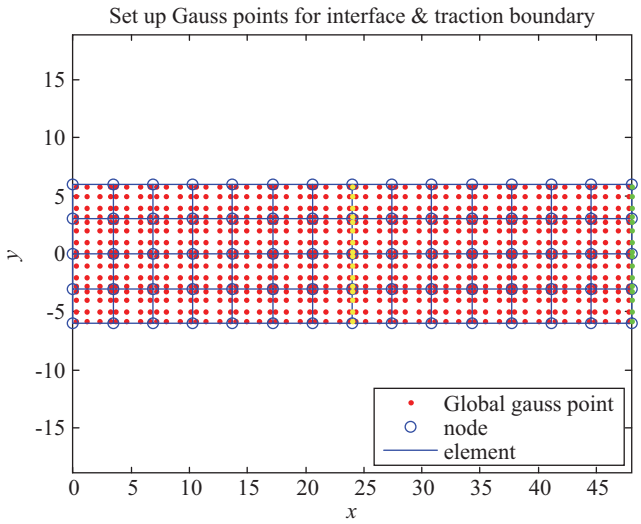

Fig. 21. Set up Gauss point for interface and traction boundary of composite beam.

Thus the responses obtained in Figs. 20 and 21 can be directly compared with the results presented in [15, 20]. Here again, a very good agreement can be found. Furthermore, it can be observed in Fig. 22 that the amplitude decreases as the time increases from 0 to 1.0 s. The response oscillates in a steady state way after 1.0 s because damping affect is ignored in the system. On the other hand, a damping in the system results an amplitude decrease to zero as the time increases, as illustrated in Fig. 19. Very stable results for the forced vibration analysis are obviously achieved by the present meshfree method.

The offshore structure is modeled with mesh free while the soil domain is described by boundary elements instead. For both situations, the two different parts are then coupled together ensuring compatibility and equilibrium along the common interface. For the coupling itself, quite mature algorithms are available meanwhile, in fact, it can be done either in a direct way by solving a coupled system of equations or by means of an iterative coupling scheme.

If the soil domain is modeled by mesh free nodes, some kind of truncation in the soil region is necessary, as a closed domain is compulsory for the implementation of the Mfree methods. Such truncations lead to different artificial boundaries, which can reflect elastic waves generated from structural vibrations. Since in most soil-structure interaction problems the soil domain is assumed to be semi-infinite, the spurious wave reflection due to artificial boundaries may substantially deteriorate the accuracy of the computation. This phenomenon is well known as the “boxing effect” in geomechanics. A

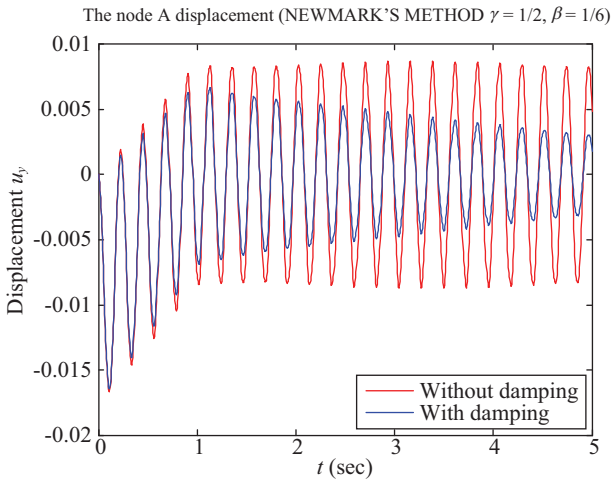

Fig. 22. Transient displacement u_y at point A without and with damping under transient loading with a finite decrease time.

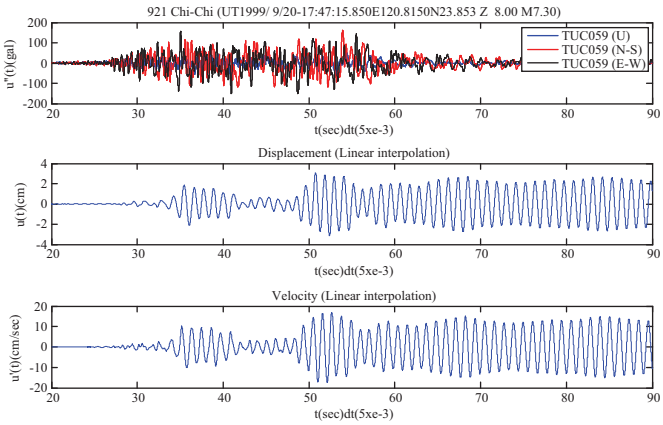

Fig. 23. Chichi earthquake motion 1999.

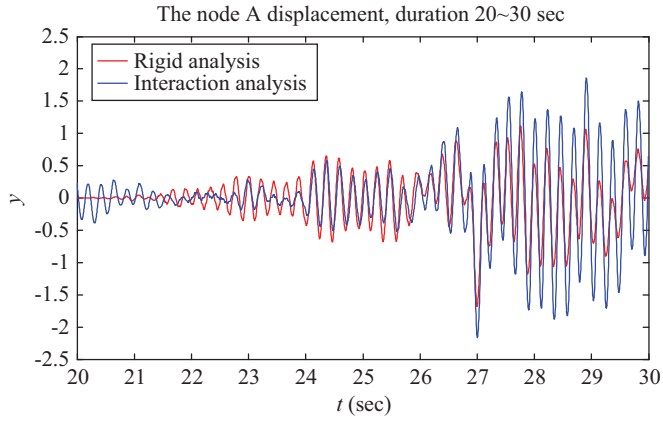

Fig. 24. Offshore structural model with time histories of the displacement at node 'A'.

number of assumptions, such as absorbing or non-reflecting boundary conditions have been proposed to modify different artificial boundaries in order to reduce the wave reflection. However, strict restriction and soaring computational effort by applying such measures make them less effective in practical applications. If boundary elements are applied to model the soil region, the dimensionality of the problem is reduced by one order and the treatment of infinite domain is straight forward.

In this study, dynamic response analysis for an ideal 2D offshore-structure with a soil-pile foundation system induced by seismic motions is performed. Fig. 14 shows an overview of the offshore structure-soil system. For mathematical modeling of the current structure, a Cartesian coordinate system was chosen such that the origin is located at a point on the sea bottom projected from the left corner of the deck plate. x is positive to the right and y is positive in the upward direction. For numerical calculation, the system is composed of discrete mesh and nodal points as shown in Fig. 16. Three nodal points A, B, C on the superstructure, as indicated in Fig. 14, were selected to calculate the respective displacement against seismic motions. The governing equation of motion for the entire structure can be formulated as (27).

In the seismic analysis, it is assumed that tanks are subjected to North-South component of the ground motion recorded at the Chin-Shui Elementary School during the September 21st, 1999 Chichi earthquake in Taiwan. To evaluate the dynamic response of the offshore structure-soil system, Three soil types shown in Table 4 were considered. Soil conditions recommended in the literature were considered in the selection of soil types and their properties. The time history analyses were carried out by using the above-mentioned system in Fig. 23.

The results of the present model are compared with and without offshore structure-soil interaction analysis. All the vertical side nodes are fitted with dashpots while the bottom nodes are considered to be rollers. The 921-Chichi earthquake acceleration is applied to the offshore structure system prototype and solved this problem by the coupled MKEFG-BEM method. They included the effect of viscous damping with a damping ratio of 0.05. Moreover, the effect of hydrodynamic pressure was incorporated in the analysis by the added mass concept proposed by Westergaard [30]. The effect of wave scattering and reflection was tackled by the present method. When the model is solved by the proposed scheme, the effect of viscous damping and the hydro- dynamic pressure is also considered in similar way. Also, initially the dam has been analyzed considering the effects of itself weight and the hydrostatic pressure which produced initial acceleration in the system. Fig. 24 shows the comparison between the variation of node A displacements, obtained with and without offshore structure-soil interaction analysis during 20~30 sec. The maximum and minimum values of the horizontal displacements for the interaction analysis are found to be 1.92 cm and -2.27 cm respectively, while those for rigid analysis are 1.12 cm and -1.83 cm. Fig. 25 shows the comparison between the variations of bending stresses at all nodal points for rigid and interaction analysis. A maximum value of 119.98 MPa is

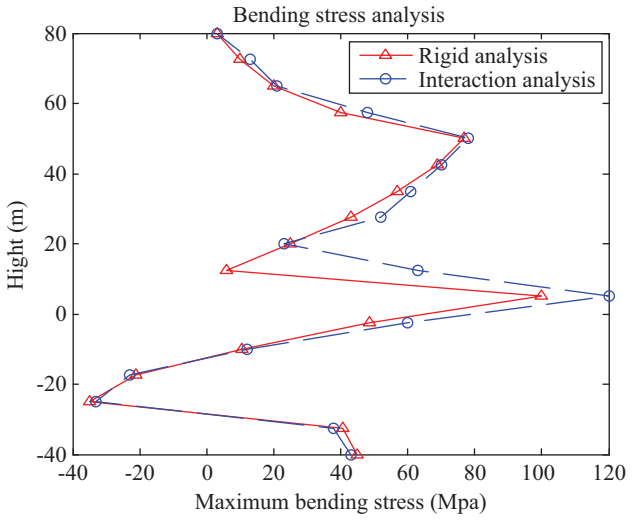

Fig. 25. Offshore structural model with time histories of maximum bending stresses at all nodal points.

obtained with interaction analysis while the maximum value for rigid analysis is found to be 100.39 MPa. It is evident from the above observations that the displacements have increased for interaction analysis compared to the rigid case. Also, the stresses at the pile head zone have increased when the flexibility effect of pile-soil system is taken care in the coupled analysis. Since the bottom mounted platform region to the head of the pile experiences more stresses compared to the stresses observed at the tip 43.66 Mpa, therefore the stresses obtained from offshore structure-soil interaction analysis should govern design criteria of the offshore structure system.

The results of the present model are compared with and without offshore structure-soil interaction analysis. All the vertical side nodes are fitted with dashpots while the bottom nodes are considered to be rollers. The 921-Chichi earthquake acceleration is applied to the offshore structure system prototype and solved this problem by the coupled MKEFG-BEM method. They included the effect of viscous damping with a damping ratio of 0.05. Moreover, the effect of hydro-dynamic pressure was incorporated in the analysis by the added mass concept proposed by Westergaard [30]. The effect of wave scattering and reflection was tackled by the present method. When the model is solved by the proposed scheme, the effect of viscous damping and the hydro-dynamic pressure is also considered in similar way. Also, initially the dam has been analyzed considering the effects of itself weight and the hydrostatic pressure which produced initial acceleration in the system. Fig. 24 shows the comparison between the variation of node A displacements, obtained with and without offshore structure-soil interaction analysis during 20~30 sec. The maximum and minimum values of the horizontal displacements for the interaction analysis are found to be 1.92 cm and -2.27 cm respectively, while those for rigid analysis are 1.12 cm and -1.83 cm.

Fig. 25 shows the comparison between the variations of

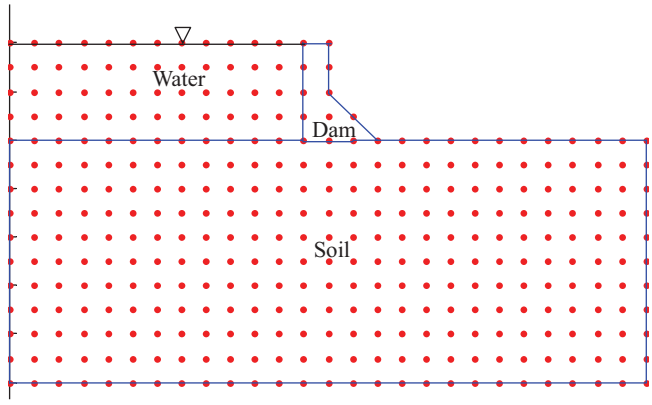

Fig. 26. The geometry of dam-foundation prototype.

bending stresses at all nodal points for rigid and interaction analysis. A maximum value of 119.98 MPa is obtained with interaction analysis while the maximum value for rigid analysis is found to be 100.39 MPa. It is evident from the above observations that the displacements have increased for interaction analysis compared to the rigid case. Also, the stresses at the pile head zone have increased when the flexibility effect of pile-soil system is taken care in the coupled analysis. Since the bottom mounted platform region to the head of the pile experiences more stresses compared to the stresses observed at the tip 43.66 Mpa, therefore the stresses obtained from offshore structure-soil interaction analysis should govern design criteria of the offshore structure system.

A dam in Fig. 26 of height 15.0 m, crest-width 2.0 m and base width 10.0 m discretized with isoparametric linear quadric lateral elements. This particular dam-foundation system was originally solved by Yazdchi *et al.* [34] using coupled FEM-BEM technique considering soil-structure interaction effects. While solving the dam-foundation interaction problem, the side nodes of the discretized finite elements in the foundation portions were considered to be connected to dashpots allowing only the horizontal movements and the bottom nodes were considered to be rollers. The middle node at the base of the foundation is kept fixed in order to prevent rigid body translation in the x direction. A 2×2 Gauss Integration rule is adopted for the calculation of both the stiffness matrix and the mass matrix. The dam and the foundation are assumed to be linear elastic with the following material properties. Poisson's ratio 0.2; modulus of elasticity $E = 3 \times 10^7$ kN/m^2 and mass density as 2600 kg/m^3. The Poisson's ratio and the mass density of the foundation were assumed to be the same as those of the dam.

The maximum crest displacement of the dam under seismic excitation (Fig. 27) by both the method has been tabulated in the Table 5 for a comparison purpose. The present results are also compared with the results obtained by Reddy *et al.* [25]. The obtained displacements by the proposed interaction scheme are in very close agreement with the results obtained both by Yazdchi *et al.* [34] and Reddy *et al.* [25].

Table 5. Comparison of maximum horizontal crest displacements (mm).

Horizontal crest displacements (mm)	Coupled FE-BE solution Yazdchi *et al.* [34]	Reddy *et al.* [25]	Proposed method
Impedance ratio(E_f/E_d)			
0.5	6.89	8.60	6.77
	-7.53	-	-8.71
1.0	4.38	4.60	4.92
	-4.41	-	-5.25
2.0	4.27	4.50	4.56
	-3.85	-	-5.13
4.0	4.11	3.90	4.13
	-3.70	-	-4.77

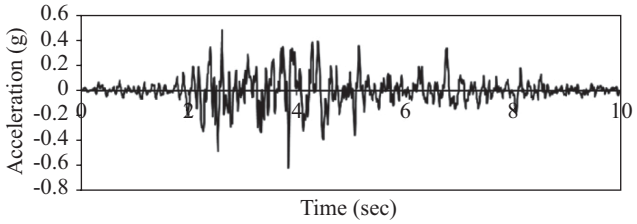

Fig. 27. Koyna earthquake motion 1967.

VI. CONCLUSION

Since seismic motions may cause serious damage to a bottom mounted platform, the effects of earthquakes on the dynamic response of the structure should be scrutinized in order to design reliable structures in seismic zones. This paper presents a methodology for the analysis of offshore structural system subjected to seismic excitations considering the soil-structure interaction effect. The proposed method is validated from the literature which shows the accuracy of the developed algorithm. The offshore system like structure, having the coupling effect due to the soil-pile foundation material during earthquake excitations is analyzed. The numerical results presented here prove the efficiency of the present algorithm to solve a soil-structure coupled problem of massive structures such as the typical offshore system. The advantage of using the present MKEFG-BEM method is that it requires less computational effort, in terms of both time and memory. The responses of the soil-structure system considering an absorbing boundary indicate that the incident energy is effectively absorbed at the truncation boundary. Another advantage of this method is that it requires less computational effort since it avoids evaluation of convolution integrals and Fourier transforms to calculate soil-structure interaction forces. The algorithm presented here is simple so that it may be programmed easily. The results show that the displacements and stresses have increased for the elastic as compared to the rigid base. Hence it is advisable to carry out the interaction analysis for pile structures like offshore under flexible base. It is also observed that the pile head is the most severely stressed zone; hence one may expect the appearance of cracks around the pile head region of the offshore structure system.

The model used in the current study is illustrated in Fig. 14, and Table 2 lists its properties. Table 3 shows the respective natural periods of the present platform for various soil conditions. The natural period of the platform decreased as the shear-wave velocity of the soil increases (i.e., as soil becomes harder). Therefore, the dynamic behavior of the present system is directly dependent on soil conditions. The dynamic response of the structure was calculated using a time history of the most severe seismic waves. Fig. 23 shows the time histories of displacement at node A for the seismic motions given in Fig. 24 The maximum acceleration and the shearwave velocity of the soil (Vs) were adjusted to 156 Gal and 100 m/s, respectively. It is observed that the displacement of the fixed foundation system was relatively small compared to that of the pile-soil foundation system, due to less structure-soil interaction. Since platform motion is significantly influenced by seismic frequency, the maximum response induced by interaction analysis was greater than that induced by rigid case. The patterns of displacement differ greatly in the slow shear velocities, and variations in time histories converge at high velocities (e.g., 500 m/s). Since the body responses show similar patterns in firm soil conditions for both seismic motions, it is found that displacement in the pile-soil foundation system was influenced more by soil condition than by the magnitude of the seismic motions. Fig. 25 shows because the structure bottom is influenced by the soil conditions; thus, the bending stress at the bottom is reduced in soft soil conditions due to the large displacement.

The capability of equation solver has been significantly improved with the advances of computer science. Many problems traditionally considered to be ill-conditioned, now can be accurately calculated without difficulty by using the proposed MK-EFGM-BEM together with the analysis of condition number. A more systematic study on the accuracy and condition number for the MK-EFGM deserves further investigation. The further details of a method may be obtained from picking the reference from the exhaustive list presented in the paper [19, 26].

ACKNOWLEDGMENTS

This research has been financially supported in part by the NSC of ROC (Taiwan) under grants “NSC-101-2221-E-110-108”. The financial support is gratefully appreciated. We would like to thank the reviewers for suggesting very constructive comments which helped improve our paper. It is greatly appreciated.

REFERENCES

1. Atluri, S. N., *The Meshless Local Petrov-Galerkin (MLPG) Method*, Tech Science Press (2004).

2. Aydinoglu, M. N., "Development of analytical techniques in soil structure interaction, in development in dynamic soil structure interaction," in: Gulkan, P. and Clough, R. W. (Eds.), *Proceedings of the NATO Advanced Study Institute*, Kluwer Academic Publishers, Kemer, Antalya, Turkey, pp. 25-42 (1993).
3. Bathe, K. J., *Finite Element Procedures*, Prentice-Hall, Englewood Cliffs, New Jersey (1996).
4. Bea, R. G., "Earthquake and wave design criteria for offshore platform: evaluations of modal solutions," *Engineering Structures*, Vol. 108, pp. 2175-2191 (1979).
5. Belytschko, T. and Lu, Y. Y., and Gu, L., "Element free Galerkin method," *International Journal for Numerical Methods in Engineering*, Vol. 37, pp. 229-256 (1994).
6. Bode, C., Hischauer, R., and Savidis, S. A., "Soil-structure interaction in the time domain using halfspace Green's functions," *Soil Dynamic and Earthquake Engineering*, Vol. 22, pp. 283-295 (2002).
7. Bui, T. Q., *Application of the Element Free Galerkin Method for Dual Analysis*, European Master's Thesis, University of Liege, Belgium (2005).
8. Bui, T. Q. and Nguyen, M. N., "A moving Kriging interpolation-based meshfree method for free vibration analysis of Kirchhoff plates," *Computer and Structures*, Vol. 89, pp. 380-394 (2011).
9. Bui, T. Q. and Nguyen, T. N., and Nguyen-Dang, H., "A moving Kriging interpolation-based meshless method for numerical simulation of Kirchhoff plate problems," *International Journal for Numerical Methods in Engineering*, Vol. 77, pp. 1371-1395 (2009).
10. Bui, T. Q. and Nguyen-Dang, H., "An equilibrium model in the element free Galerkin method," *The Eight International Conferences on Computational Structures Technology*, Las Palmas de Gran Canaria, Spain, 12-15 September (2006).
11. Chang, P.-Y., Lee, H. H., Tseng, G. W., and Chung, P. Y., "VFIFE method applied for offshore template structures upgraded with damper system," *Journal of Marine Science and Technology*, Vol. 18, No. 4, pp. 473-483 (2010).
12. Dai, K. Y. and Liu, G. R., "Free and forced vibration analysis using the smoothed finite element method (SFEM)," *Journal of Sound and Vibration*, Vol. 301, pp. 803-820 (2007).
13. Gu, L., "Moving Kriging interpolation and element free Galerkin method," *International Journal for Numerical Methods in Engineering*, Vol. 56, pp. 1-11 (2003).
14. Gu, Y. T. and Liu, G. R., "A meshless local Petrov-Galerkin (MLPG) method for free and forced vibration analyses for solids," *Computational Mechanics*, Vol. 27, pp. 188-198 (2001).
15. Gu, Y. T. and Liu, G. R., "A meshfree weak-strong form (MWS) method for time dependent problems," *Computational Mechanics*, Vol. 35, pp. 134-145 (2005).
16. Hughes, T., *The Finite Element Method - Linear Static and Dynamic Finite Element Analysis*, Prentice Hall, Englewood Cliffs, New Jersey (1987).
17. Karadeniz, H., "Reliability calculation of RC offshore structures inter extreme wave loading," *Proceedings of the Fifteenth International Off-Shore and Polar Engineering Conference*, pp. 399-406 (2005).
18. Lam, K. Y., Wang, Q. X., and Li, H., "A novel meshless approach - Local Kriging (LoKriging) method with two-dimensional structural analysis," *Computational Mechanics*, Vol. 33, pp. 235-244 (2004).
19. Lee, H. H., "Seismic and vibration mitigation for the a-type offshore template platform system," *Structural Engineering and Mechanics*, Vol. 6, No. 3, pp. 347-362 (1998).
20. Li, H., Wang, Q. X., and Lam, K. Y., "Development of a novel meshless Local Kriging (LoKriging) method for structural dynamic analysis," *Computer Methods in Applied Mechanics and Engineering*, Vol. 193, pp. 2599-2619 (2004).
21. Liu, G. R., *Meshfree Methods, Moving Beyond the Finite Element Method*, CRC Press, U.S.A. (2003).
22. Lysmer, J. and Kuhlemeyer, R. L., "Finite dynamic model for infinite media," *Journal of Engineering Mechanics Division*, ASCE, Vol. 95 (EM4), pp. 859-877 (1969).
23. Park, M. S., Koo. W., and Kawano, K., "Dynamic response analysis of an offshore platform due to seismic motions," *Engineering Structures*, Vol. 33, pp. 1607-1616 (2011).
24. Penzien, J., Kaul, M. K., and Berge, B., "Stochastic response of offshore towers to random sea waves and strong motion earthquake," *Computer and Structures*, Vol. 2, pp. 733-59 (1972).
25. Reddy, B. V., Burman, A., and Maity, D., "Seismic response of concrete gravity dams considering foundation flexibility," *Indian Geotechnical Journal*, Vol. 38, pp. 187-203 (2008).
26. Rizos, D. C. and Wang, Z., "Coupled BEM-FEM solutions for direct time domain soil- structure interaction analysis," *Engineering Analysis with Boundary Elements*, Vol. 26, pp. 877-888 (2002).
27. Sayakoummane, V. and Kanok-Nukulchai, W., "A meshless analysis of shells based on moving Kriging interpolation," *International Journal of Computational Methods*, Vol. 4, pp. 543-565 (2007).
28. Tongsuk, P. and Kanok-Nukulchai, W., "On the parametric refinement of moving Kriging interpolations for element free Galerkin method," *Computational Mechanics WCCM VI in Conjunction with APCOM'04*, Septembeer 5-10, Beijing, China (2004).
29. Tongsuk, P. and Kanok-Nukulchai, W., "Further investigation of element free Galerkin method using moving Kriging interpolation," *International Journal of Computational Methods*, Vol. 1, pp. 1-21 (2004).
30. Westergaard, H. M., "Water pressures on dams during earthquakes," *Transactions of the ASCE*, Vol. 98, pp. 418-433 (1933).
31. White, W., Valliappan, S., and Lee, I. K., "Unified boundary for finite dynamic models," *Journal of Engineering Mechanics Division*, ASCE, Vol. 103, pp. 949-964 (1977).
32. Wolf, J. P., *Soil Structure Interaction Analysis in Time Domain*, Prentice Hall, Inc., Englewood Cliffs, New Jersey (1988).
33. Yamada, Y., Kawano, K., Iemura, H., and Venkataramana, K., "Wave and earthquake response of offshore structure with soil-structure interaction" *Proceeding of JSCE, Structure Engineering and Earthquake Engineering*, Vol. 5, No. 2, pp. 361-370 (1988).
34. Yazdchi, M., Khalili, N., and Valliappan, S., "Dynamic soil-structure interaction analysis via coupled finite element-boundary element method," *Soil Dynamics and Earthquake Engineering*, Vol. 18, pp. 499-517 (1999).